RSC Advances

ROYAL SOCIETY OF CHEMISTRY

www.rsc.org/advances

Fast & Scalable Pattern Transfer *via* Block Copolymer Nanolithography

Tao Li,[a] Zhongli Wang,[ab] Lars Schulte,[ab] Ole Hansen,[ac] and Sokol Ndoni*[ab]

[a]Department of Micro- and Nanotechnology, Technical University of Denmark, DK-2800 Kgs. Lyngby, Denmark.

[b]Center for Nanostructured Graphene (CNG), Technical University of Denmark, DK-2800 Kgs. Lyngby, Denmark.

[c]Center for Individual Nanoparticle Functionality (CINF), Technical University of Denmark, DK-2800, Kgs. Lyngby, Denmark

*To whom correspondence should be addressed. E-mail: sond@nanotech.dtu.dk (S. N.)

ABSTRACT:

A fully scalable and efficient pattern transfer process based on block copolymer (BCP) self-assembling directly on various substrates is demonstrated. PS-rich and PDMS-rich poly(styrene-*b*-dimethylsiloxane) (PS-*b*-PDMS) copolymers are used to give monolayer sphere morphology after spin-casting of solutions with selective solvents relative to the majority block. The pattern is directly formed during spin-casting at room temperature, which takes less than 20 seconds, without any preliminary surface treatment of the substrate and without any subsequent annealing. The self-assembled BCPs are transformed into hard lithography masks by oxidation of PDMS in

oxygen plasma. The hard masks are then used to fabricate full wafer scale arrays of nano-pillars and nano-wells on various substrates, including polymers and silicon. The demonstrated BCP nanolithography process opens up for numerous applications not relying on long range lateral order, including fabrication of substrates for catalysis, solar cells, sensors, ultrafiltration membranes and templating of semiconductors or metals.

Introduction:

Pattern transfer at nano-scale is a key process in nanotechnology. Challenges arise from the increasing cost and limited resolution of top-down approaches like deep-UV optical lithography. On the other hand, the low throughput e-beam lithography and interference techniques are not suitable for efficient large area patterning.[1] Self-assembly of block copolymers can result in highly ordered nanostructures with varying morphology on sub-10 nm scale, making it a promising technique to meet the key challenges of small feature size with high resolution and high throughput at low cost.[2, 3] Various BCP patterns with narrow size distribution and perfect alignment have been created so far.[4-7] However, there is still a need for a facile and versatile approach using block copolymers with large etching contrast and substrate independence to succeed in a number of applications where the perfect lateral ordering of the nano-pattern is not necessary such as solar cells, catalysis, separating membranes, plasmonic substrates, etc.

When BCP films are spin-cast, they are often kinetically trapped in disorganized form far from the equilibrium state. Therefore an annealing process, such as thermal annealing[8] and solvent vapor annealing[9], is generally needed to generate structural order by increasing the chain mobility and allowing for BCP micro-domain separation. The annealing step indeed increases

the complexity and cost of fabrication, and some aspects of these processes might be challenging to implement in industry. In addition to the annealing process, the substrates have to be treated prior to BCP deposition in nearly all the BCP lithography studies. For an example, by applying a random copolymer with controlled composition covalently bonded to the substrate, a so called brush layer, a neutral surface energy for both of the polymers can be adjusted so the BCP orientation can be aligned normal to the substrate.[10] This approach, however, requires anchoring chemical groups present both in the substrate and brush polymer, which limits its applications. Other examples including homo-polymer brush layer,[11] or substrate chemical functionalization,[12] are routinely applied to increase the BCP chain mobility, prevent de-wetting or control the orientation.

Another challenge for BCP nanolithography is to use block copolymers with high Flory–Huggins interaction parameter (χ), which improve the ordering quality, reduce defect level and allow to fabricate patterns with smaller feature sizes and periods. So far, poly(styrene-*b*-methyl methacrylate) (PS-*b*-PMMA) is the most investigated BCP system due to the easy removal of the PMMA block under UV illumination. But the low χ ($\chi_{PS\text{-}PMMA} \sim 0.06$ at 25^{o}C) of this BCP reduces the possibility of reaching sub-20 nm features and the remaining PS has a low etching resistance under reactive ion etching (RIE), making it a poor mask for a pattern transfer process. One major route to increase χ and generate hard masks is to incorporate an inorganic domain which is highly incompatible with the organic block.[13] For example, PS-*b*-PDMS (SD) attracts intensive research interest due to its high segregation strength ($\chi_{PS\text{-}PDMS} \sim 0.27$ at 25^{o}C) and large etching contrast. [14, 15] Under oxygen plasma, the PDMS block is converted to silicon oxy carbide

while the PS block is etched away, leaving a hard mask with much enhanced thermal stability and mechanical strength. [13, 16]

Fast pattern generation directly after spin-casting has been reported for poly(styrene-*b*-ethylene oxide) (PS-PEO)[17, 18] and poly(styrene-*b*-lactide) (PS-PLA)[19, 20] with perpendicular cylindrical morphology. The evaporation rate and solubility parameter of the solvents play a key role in determining the microdomain orientation. However, the PEO block cannot be removed easily by chemical etching.[21] In the case of PS-PLA, if the PLA domain is removed by hydrolysis with a base, the remaining PS is a poor mask for a pattern transfer process. Deposition of block copolymer micelles from selective solvents can produce nano-pattern directly on the substrates,[22] but the casting conditions are rather delicate.[23, 24] In order to improve the etching resistance of the mask, an extra step of inorganic precursor infiltration is applied prior to the nano-pattering process.[23, 25, 26] PS-PDMS is also reported for a similar purpose;[27] however, the pattern transfer involves tedious mask transfer which is less attractive for mass production.

Here we introduce a large-scale and facile pattern transfer process by in situ block copolymer nanolithography. The in situ PS-PDMS pattern is realized from selective solvent spin-casting, giving a monolayer sphere morphology, which allows avoiding the vertical orientation control for nano-patterning. We successfully transfer the pattern to various substrates including common polymers and silicon, without any substrate pretreatment and annealing steps. In a very recent publication we have demonstrated formation and transfer of nanopatterns with highly regular lateral order created from PDMS-rich PS-PDMS block copolymers directly applied on many

important substrates with widely varying surface energies.[28] Vapor solvent annealing with solvents selective to PDMS was applied in that study.

Methods:

Materials: All the solvents are purchased from Sigma Aldrich without further purification (except for the BC synthesis). SD67 (21-b-46 kg mol^{-1}, Polymer Source), SD81 (26-b-55 kg mol^{-1}, Polymer Source), SU8-2002 (MicroChem), Poly(methyl methacrylate) (PMMA, 70k, Diakon), Polysulfone (PSF 27k, Scientific Polymers), Polylactide (PLA M_w 18k-28k, Sigma Aldrich) and 1, 4-polybutadiene (PB Scientific Polymers, *MW* 100k, crosslinking procedure:[29]) are used as received. SD39 and SD23 are synthesized by living anionic polymerization following already reported procedures.[30]

Fabrication: All the SDs with concentration of 0.3 wt% to 0.5 wt% were spin-cast at 1500 rpm for 20 seconds to give 12 – 22 nm thick films. SU8 (7 wt% in Cyclopentanone) was spin-cast at 5000 rpm for 30 seconds to give a 110 nm thick film, and then cross-linked onto a hot plate at 250 ^{o}C for 15 minutes.

The dry etch process was performed in an Advanced Silicon Etcher (ASE, STS MESC Multiplex ICP serial no. 30343). SF_6 plasma conditions to remove the PDMS top wetting layer: 20 sccm SF_6 flow rate, 20 mTorr pressure, 50 W coil power and 0 W platen power for 8 – 20 seconds. O_2 plasma condition to remove PS/polymer substrate and oxidize PDMS: 10 sccm O_2 flow rate, 5 mTorr pressure, 200 W coil power and 10 W platen power. The etch rate of the SU8 was estimated to be 3 nm/s as measured by ellipsometry. SF_6 plasma condition for breakthrough of

the PDMS-substrate wetting layer: 20 sccm SF_6 flow rate, 5 mTorr pressure, 100 W coil power and 5 W platen power for 3 seconds. The silicon etching by fluorine RIE was performed in the ASE with the parameters: 10 sccm SF_6 flow rate, 5 mTorr pressure, 100 W coil power and 5 W platen power for 10-25 seconds. The silicon etching in a pseudo-Bosch process was performed in an ICP tool (SPTS Serial number MP0637). Recipe: 38sccm SF_6 and 70sccm C_4F_8 flow rates, 14 mTorr pressure, 200 W coil power and 20 W platen power for 10 to 20 seconds.

Characterization: ^{1}H-NMR was done in deuterated chloroform, using a 400 MHz NMR from Bruker. Size exclusion chromatography was done using THF as an eluent. The system from Shimadzu, LC-10AD (Pump), SIL-10AS (Autosampler), was combined with Detectors from Viscotek, namely a RALLS Detector (Model LD600) as well as a Differential Refractometer/Viscometer (Model 200) combination. The columns were: one PLgel 5 μm Mixed D from Polymer Laboratories in series with one Styragel HMW 6E from Waters. The molecular weight of the PS block of the polymers was determined using the Refractive Index signal in combination with a conventional calibration against PS standards. The calculations of the polydispersity index (PDI) for the BCs was done by analyzing the combined Light Scattering and Refractive Index responses. The block copolymer solutions used in spin-casting were characterized by dynamic light scattering, DLS, in a Brookhaven Instruments Corporation instrument, consisting of a BI-200SM goniometer, a BI-APD detector and a 633 nm laser (Melles Griot, 25-LHP-928-249); the scattered light was collected at 90º and the data were analyzed by Dynamic light scattering software from Brookhaven Instruments, vers. 5.9. Film thicknesses were determined using a VASE Ellipsometer (J. A. Woollam) at three different incidence angles (55^o, 60^o and 65^o). Scanning electron microscopy (SEM) images were taken using a Field Emission Zeiss Ultra Plus scanning electron microscope with a Gemini column

operating at an accelerating voltage of 2 kV. The cross-section images were taken at a tilt angle of 45º. All samples were imaged directly without coating or staining. XPS measurements were performed on a XPS-ThermoScientific instrument.

Results and discussion

Four SDs with different number-average molecular weights (M_n) and composition were investigated, as summarized in Table 1. The PS volume fraction was close to 30% or 65%, corresponding to PS cylinders in a PDMS matrix or vice versa. SD23 and SD39 were synthesized in our lab by living anionic polymerization with a low polydispersity index (PDI ≤ 1.03). SD67 and SD81 were purchased with somewhat higher PDI.

Table 1. PS-b-PDMS copolymer characteristics

Sample ID	f_{PS}	M_{PS} (kg/mol)	M_{Total} (kg/mol)	PDI
SD23	64.8% [a]	15.9 [b]	23.1 [c]	1.02 [d]
SD39	66.1% [a]	27.2 [b]	38.9 [c]	1.03 [d]
SD67	29.7% [a]	21.0 [e]	67.0 [e]	1.45 [e]
SD81	30.4% [a]	26.0 [e]	81.0 [e]	1.25 [e]

[a] Calculated from ^{1}H NMR spectra using ρ_{PDMS} = 0.97 g/cm^3 and ρ_{PS} = 1.05 g/cm^3.

[b] From SEC analysis calibrated with PS standards.

[c] Calculated from f_{PS} and M_{PS} .

[d] From SEC analysis of the combined RI and LS signals.

[e] From the supplier (Polymer Source).

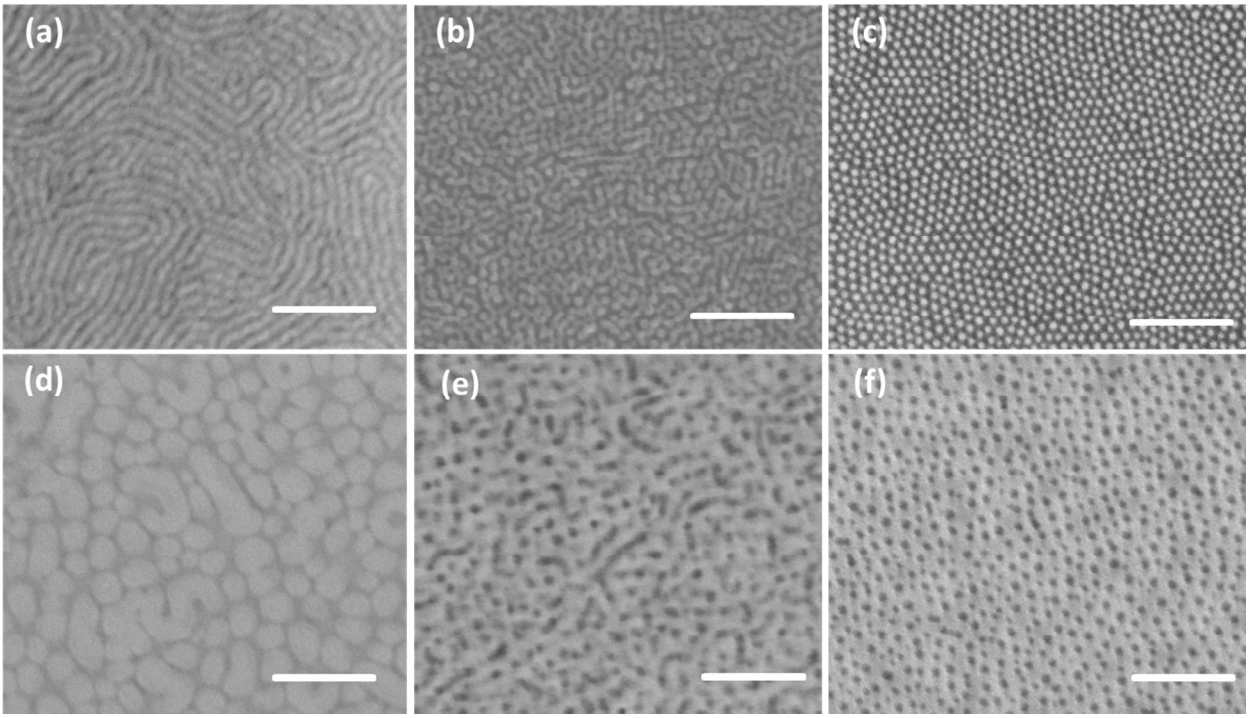

Fig. 1. Top view SEM images of the SDs after spin-casting: (a-c) PS-rich SD39 spin-cast from (a) toluene, (b) tetrahydrofuran and (c) cyclopentanone with thicknesses in the range of 15-20 nm; (d-f) PDMS-rich SD67 spin-casting from (d) toluene, (e) methylcyclohexane and (f) hexane with the thicknesses around 20 nm. All the samples were spin-cast on a silicon wafer and treated in fluorine and oxygen plasmas to enhance contrast. Scale bars: 200 nm.

Preferential inclusion of the solvent to one block of the BCP is well known to shift the morphology.[31-33] The interaction between the solvent and polymer can be considered in terms of Hildebrand solubility parameters (HSP), which are summarized in Table 2 for all the solvents used in this study. Fig. 1 shows the pattern of the SD39 and SD67 on silicon substrates after spin-casting from several solvents. For the PS-rich SD39 shown in Fig. 1a to Fig. 1c, the morphology changes from cylinder to sphere when the casting solvent changes from neutral (toluene)[34] to highly PS-selective (cyclopentanone). An intermediate state consisting of both lines and dots is also captured by tetrahydrofuran which has a HSP value in between those of

toluene and cyclopentanone. The morphology in Fig. 1c is a monolayer of hexagonally packed spheres with lateral domain size around 200 nm. A similar trend is observed for PDMS-rich SD67 shown in Fig. 1e-f, although the morphology transition to a monolayer of spheres is less evident compared to SD39. We suspect the difference is due to the limited mobility of the glassy PS-chain when cast in a non-solvent for PS, accentuated by the bigger molecular weight of SD67. In the case of SD39, the rubbery nature of the PDMS makes it easier to self-assemble into more regular pattern. The sphere morphology is clear for SD67 but the lateral order is completely missing, which may be due to its larger PDI. Moreover, defects in the film cast from neutral or less selective solvents are readily visible. In contrast, the film is very uniform and homogeneous when cast from the highly selective solvents. The thickness of the final film is smaller than the corresponding sphere packing period, as will be discussed in relation to Table 3. When a thicker film is cast, multi-layers of spheres are observed. (Fig. S1, supporting information)

Table 2. Solubility parameters (*)(**)

Solvent	Solubility parameter ($MPa^{1/2}$)
Hexane	14.9
Methylcyclohexane	16.2
Toluene	18.2
Tetrahydrofuran	18.6
Cyclopentanone	20.7
PDMS	15.0 [35]
PS	18.5 [11]

(*) Solvent values were calculated from the evaporation enthalpies and molar volumes given in ref. [36]

(**) For a more correct calculation based on the Hansen's solubility parameters, please see the supporting information, Tabs. S1, S2.

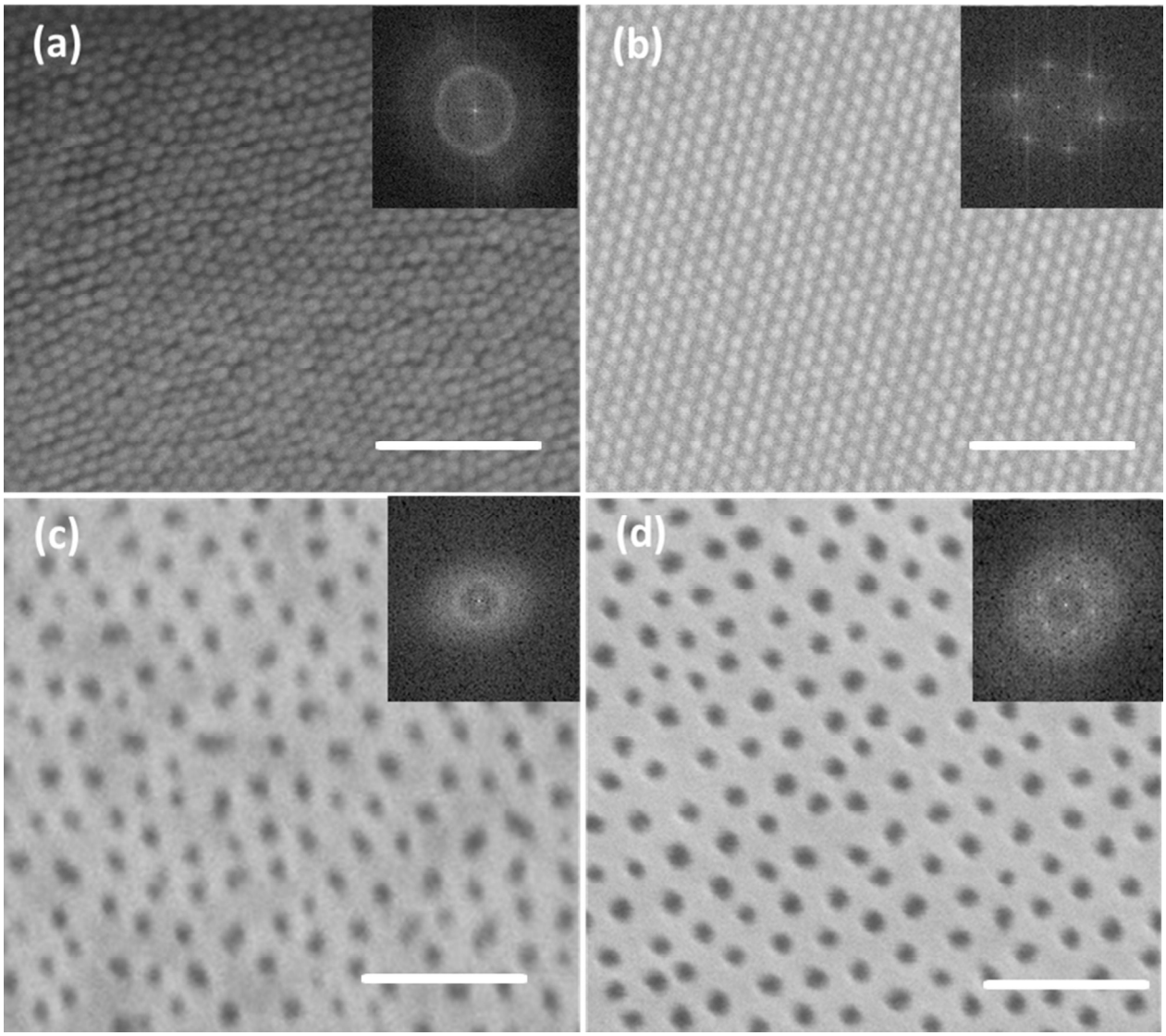

Fig 2. Top view SEM images of (a) SD23 spin-cast from cyclopentanone, (b) SD23 annealed in cyclopentanone for 1 hour, (c) SD81 spin-cast from methylcyclohexane and (d) SD81 annealed in methylcyclohexane for 1 hour. All the samples were spin-cast on a silicon wafer and treated in fluorine and oxygen plasmas to enhance contrast. Scale bars: 200 nm. Insets: Fast Fourier Transforms (FFT) of the SEM images.

The same strategy is effective for the other two SDs with different molecular weights but similar compositions, as displayed in Fig. 2a and Fig. 2c. A relatively narrow size distribution of the

nano-features is evident, even prior to the annealing step (see the discussion relative to Table 3 below). In order to improve the lateral ordering, solvent vapor annealing was applied for these two SDs. Fig. 2d and especially Fig. 2b show well-ordered morphology with lateral domain size exceeding 1 micrometer, which makes this technique attractive also for applications where lateral order is required. Based on the analysis presented in ref. [28] the annealed morphologies of figs. 2 b, d are expected to be cylindrical. This strategy could be used as a general guideline to make monolayer packed sphere patterns from bulk-cylindrical SDs with different length scale by changing the molecular weight and composition.

Dynamic light scattering of the BCPs in the spin casting solutions were recorded in order to understand the formation of the rather well-ordered structures immediately after the spin-casting step. The obtained data are shown in the second and third columns of Table 3. The effective hydrodynamic diameters measured in toluene are significantly smaller than the effective diameters in the respective selective solvents. Toluene is a good solvent for both blocks and the BCP molecules are expected to be fully dissolved; therefore the values shown correspond to hydrodynamic dimensions of single BCP macromolecules. In contrast the larger values in the selective solvents indicate formation of micelles, most probably spherical micelles for SD23, SD39, SD81 and elongated micelles for SD67. The last two columns in Table 3 show data derived from the SEM images in Figs. 1c, f and 2a, c. It has not been possible to find a clear correlation between the micelle size as measured by DLS and the structural period derived from SEM images. With the exception of SD67 the DLS micelle sizes are 2.5 – 3.6 times smaller than the corresponding thin film periods. This discrepancy hints at a reorganization of the micelles in the process of spin-casting from selective solvents. The significant shear forces during spin-casting would deform and disrupt the micelles that then reorganize before the PS block becomes

glassy as a result of solvent evaporation. The reason why SD67 forms worm-like micelles could be related to the relatively high molecular weight polydispersity of this block copolymer and to the extreme selectivity of hexane as a solvent (see Table 2). During spin-casting these micelles are also disrupted and no sign of worm-like structures remains in the thin film after spin-casting (Fig. 1f).

The standard deviations of the SEM feature sizes listed in Table 3 are moderate indicating a rather narrow feature size distribution realized by our fast process. Of course, even lower standard deviation values are realized after annealing, as is evident by inspection of Figs. 2b, d. In both these cases the standard deviation from the mean is reduced by a factor of 2.3 relative to the values for the un-annealed samples.

Table 3. Effective hydrodynamic diameter of the BCPs in non-selective and selective solvents measured by DLS together with the structural feature diameter and period measured by FFT and particle size analyses of the SEM images.

Sample ID	BCP in Toluene (nm)	BCP in selective solvents (nm)	Feature size (nm)	Period (nm)
SD23	2.3	8.1	14.0 ± 5.0	20.1
SD39	3.3	9.5	20.2 ± 3.2	34.7
SD67	7.6	83	25.8 ± 7.4	43.5
SD81	8.3	23	23.8 ± 7.0	56.6

The homogeneity over large area was examined by optical and SEM images as shown in Fig. 3. The spin-cast film is uniform across the entire surface of a 4 inch wafer (Fig. 3a). Optical microscope imaging was used to examine the absence or presence of defects such as de-wetting or formation of terraces.[33] Fig. 3b shows a random area of 4 mm by 4 mm which is seen to be defect-free. The absence of defects is also evidenced in the low and high magnification SEM

images in Figs. 3c and 3d. In contrast, a film annealed in toluene for 1 hour shows de-wetting/terrace domains, which are clearly visible in an optical microscope image (Inset in Fig. 3b). The excellent pattern homogeneity renders this method very attractive for large area patterning.

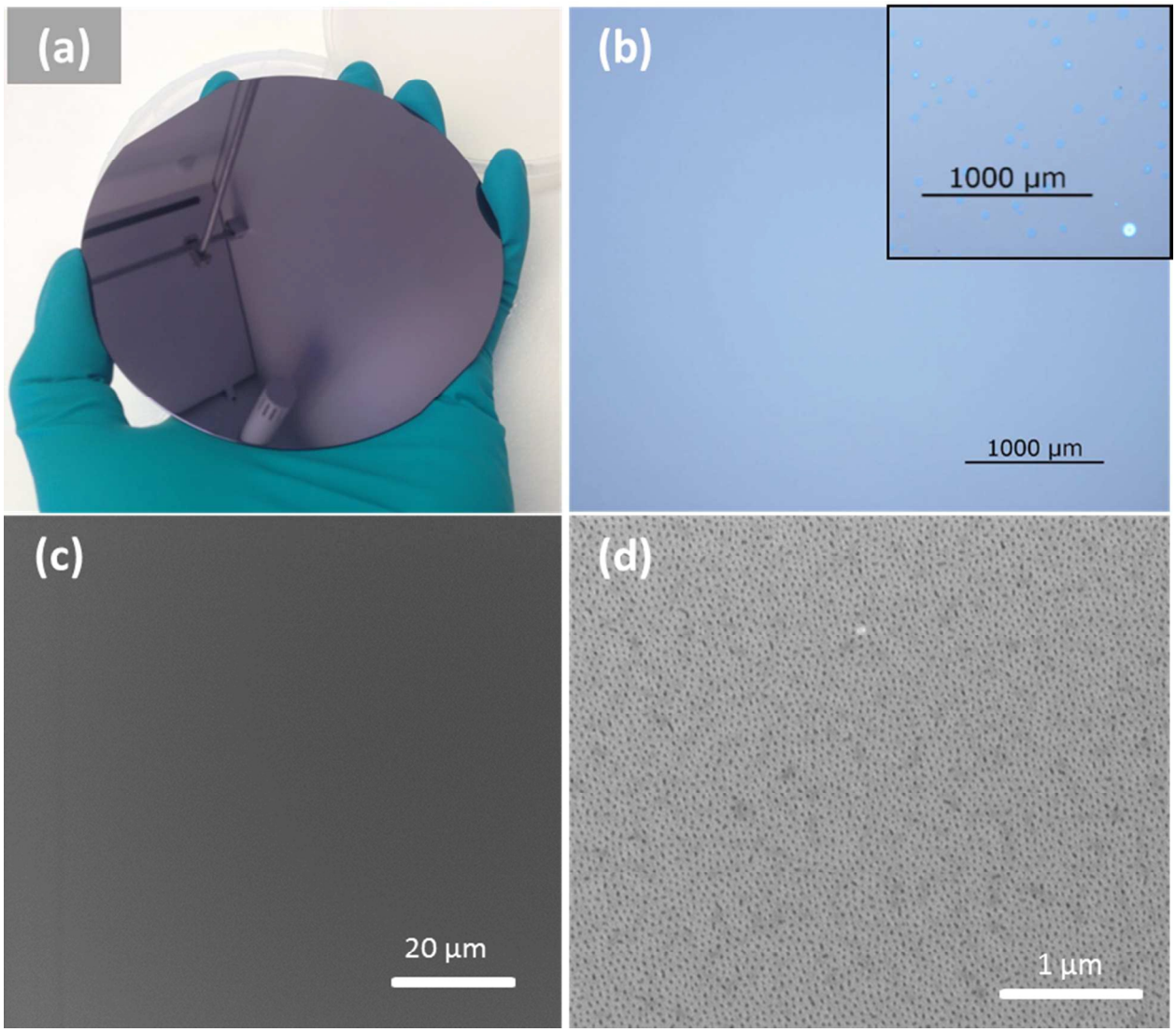

Fig. 3. (a) Photographic image of a 4 inch wafer with SD81 spin-cast on a 70 nm thick SU8 layer. (b) Optical microscope image of homogeneous SD81 film over 4 mm by 4 mm. Inset: Optical microscope image of SD81 film annealed in toluene for 1 hour, showing terraces/dewetting

formation. Low (c) and high (d) magnification SEM images of the SD81 pattern showing uniformity of the pattern.

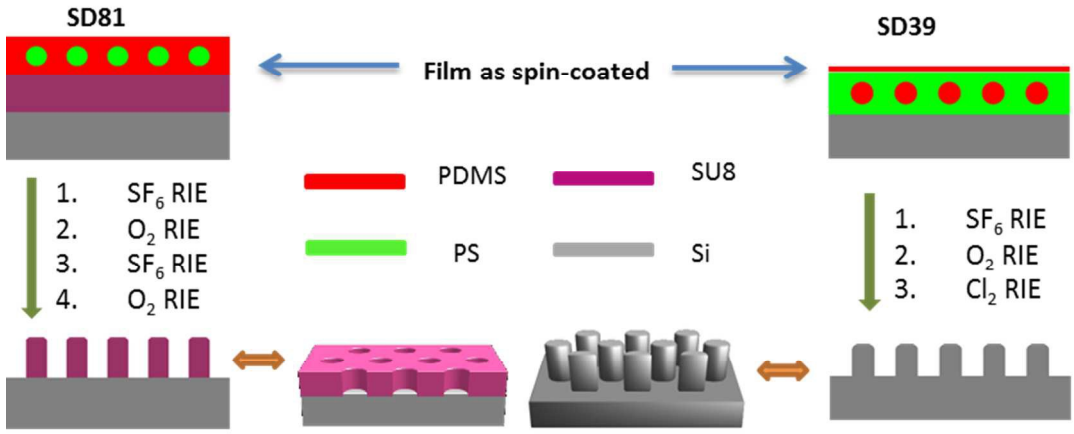

Scheme 1. Illustration of the pattern transfer processes used in this study.

The overall nano-patterning process was conducted by RIE, and the process is summarized in scheme 1. For a successful sphere pattern transfer, a short SF_6 RIE was first applied to remove a thin PDMS top wetting layer. Due to the low surface energy of PDMS compared to PS, this wetting layer of PDMS is almost always present at the air interface in SD films.[37] Then the O_2 RIE removed the PS domain and oxidized PDMS into a hard mask for the subsequent nano-patterning process. In the case of PDMS-rich SD, an additional SF_6 RIE step was needed to break through the lower PDMS wetting layer at the substrate interface. Otherwise this thin PDMS layer will block the pattern transfer during O_2 RIE (Fig. S2, supporting information). Fig. 4a and Fig. 4b show the cross-linked 110 nm thick SU8 substrate, which is a widely used photo-resist in silicon industry,[38] patterned by SD81. The obtained SU-8 nano-wells can be further used as an etching mask or as templates to fabricate other functional materials, for example, 1D nano-

rod arrays by electro-deposition or atomic layer deposition.[39, 40] Because the casting solvent – methylcyclohexane is a non-solvent for polylactide (PLA), PMMA and polysulfone (PSF), the SD81 mask works similarly on these polymer substrates, as well as on highly cross-linked polybutadiene (PB). (Fig. S3, supporting information). This technique is very attractive as an ultra-fast method for polymer patterning.

The initial attempt of pattern transfer using SD39 on polymer substrate by O_2 RIE failed (Fig. S4, supporting information). The film thickness was readily reduced as the etching proceeds but only the sphere mask can be observed. This may be due to its smaller feature size, which makes under-cutting inevitable during the dry etching process. Pattern transfer to silicon by SD39 was attempted using several fluorine-based RIE recipes, which all proved to be unsuccessful. The selectivity of the mask to the silicon substrate under these conditions is estimated to be less than 1, which suggests that the oxidized PDMS is a poor mask under SF_6 RIE. We also tested a pseudo-Bosch recipe, in which C_4F_8 gas is introduced as a passivation step to prevent undercutting in silicon etching. This recipe is deliberately designed for nanostructured silicon etching at small length scales, e.g. deep-UV lithography based processes. However, the results were discouraging. This suggests that silicon etching at very small length scales is quite challenging. Surprisingly, we find that the oxidized PDMS masks can be used not only for patterning carbonaceous materials by oxygen RIE; they also show high etch resistance over silicon under **chlorine** RIE as demonstrated by the SEM images in Fig. 4c and Fig. 4d using a SD39 mask. Unlike the isotropic oxygen plasma etching for polymer and fluorine plasma etching for silicon, the silicon etching in a chlorine plasma is highly anisotropic.[41] Therefore, regular arrays of silicon nano-pillars were obtained by direct application of chlorine plasma to the

oxidized PDMS mask. As the chlorine RIE also etches the oxidized PDMS slowly, the mask can be fully removed simultaneously, which is evidenced by the absence of the carbon peak in the X-ray photoelectron spectroscopy (XPS) spectrum. The selectivity of this mask under these conditions is estimated to be 7.

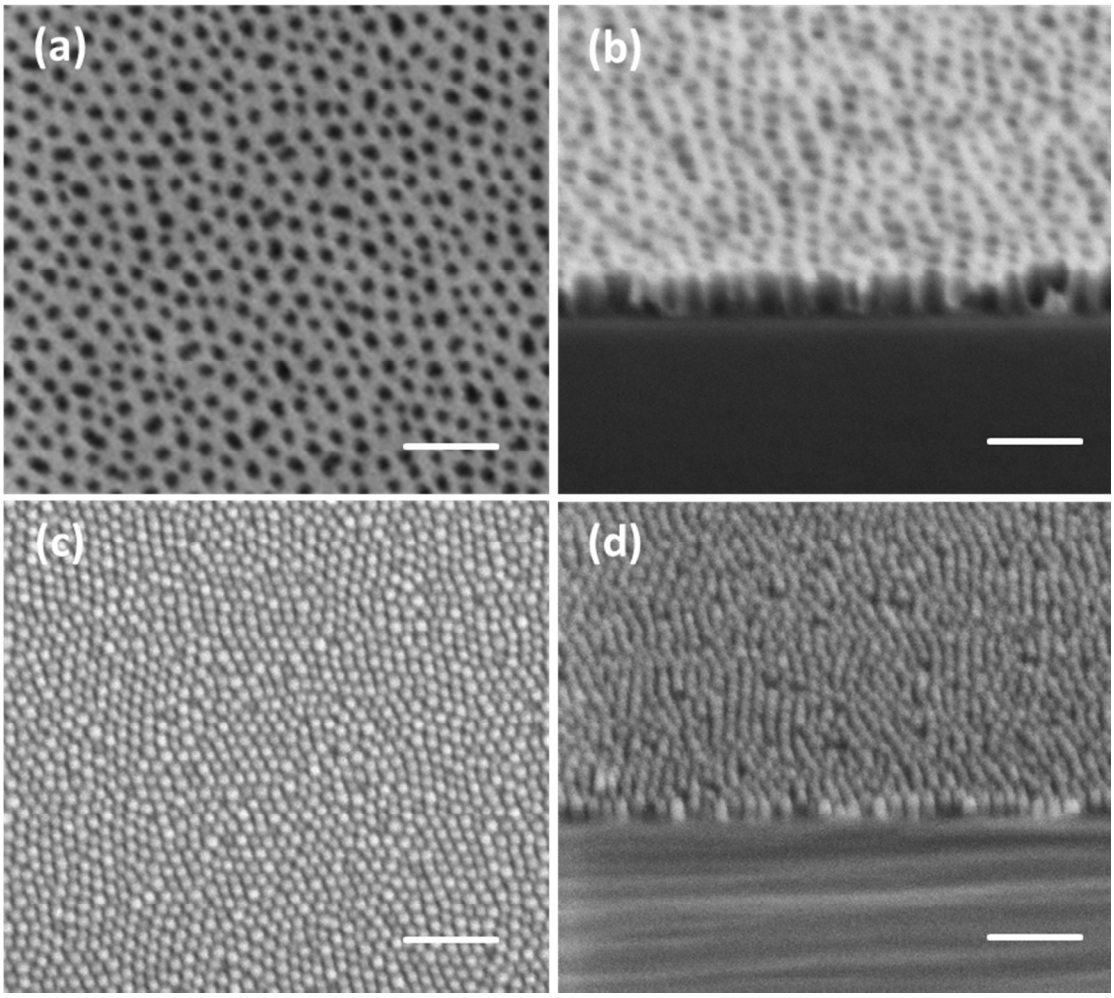

Fig. 4. Top view (a) and tilted (b) SEM images of SD81 pattern transfer into SU-8 by O_2 RIE. Top view (c) and tilted (d) SEM images of SD39 pattern transfer into silicon substrate by chlorine RIE. The SDs were directly spin-cast on the substrates without any annealing process and the transferred pattern is well replicated from the masks. Scale bars: 200 nm.

In conclusion, an extremely simple and fast BCP nanolithography process has been demonstrated on various substrates with complete coverage over wafer scale. Monolayer packed sphere morphology is kinetically captured during spin-casting using selective solvents for cylindrical SDs, with relatively low size distribution. Due to the high etching contrast between PS and PDMS domain under O_2 RIE, the pattern is successfully created and transferred to the substrates. This conceptual approach provides a powerful and facile toolset to obtain large-scale nano-patterning on various substrates without any annealing and surface modification processes, which is difficult to realize by conventional methods.

Acknowledgements

This work was supported by the Danish National Research Foundation Center for Nanostructured Graphene - CNG (DNRF58), by the Danish National Research Foundation Center for Individual Nanoparticle Functionality - CINF (DNRF54), and by the Dept. of Micro and Nanotechnology at the Technical University of Denmark.

REFERENCES

1. C. Lu and R. H. Lipson, *Laser Photonics Rev*, 2010, **4**, 568-580.
2. C. M. Bates, M. J. Maher, D. W. Janes, C. J. Ellison and C. G. Willson, *Macromolecules*, 2014, **47**, 2-12.
3. J. Bang, U. Jeong, D. Y. Ryu, T. P. Russell and C. J. Hawker, *Adv Mater*, 2009, **21**, 4769-4792.
4. X. D. Gu, I. Gunkel and T. P. Russell, *Philos T R Soc A*, 2013, **371**.
5. B. H. Kim, J. Y. Kim and S. O. Kim, *Soft Matter*, 2013, **9**, 2780-2786.
6. H. Q. Hu, M. Gopinadhan and C. O. Osuji, *Soft Matter*, 2014, **10**, 3867-3889.
7. K. Koo, H. Ahn, S. W. Kim, D. Y. Ryu and T. P. Russell, *Soft Matter*, 2013, **9**, 9059-9071.
8. H. C. Kim and T. P. Russell, *J Polym Sci Pol Phys*, 2001, **39**, 663-668.
9. C. Sinturel, M. Vayer, M. Morris and M. A. Hillmyer, *Macromolecules*, 2013, **46**, 5399-5415.

10. P. Mansky, Y. Liu, E. Huang, T. P. Russell and C. J. Hawker, *Science*, 1997, **275**, 1458-1460.
11. K. W. Gotrik, A. F. Hannon, J. G. Son, B. Keller, A. Alexander-Katz and C. A. Ross, *Acs Nano*, 2012, **6**, 8052-8059.
12. M. S. She, T. Y. Lo and R. M. Ho, *Acs Nano*, 2013, **7**, 2000-2011.
13. A. Nunns, J. Gwyther and I. Manners, *Polymer*, 2013, **54**, 1269-1284.
14. T. Nose, *Polymer*, 1995, **36**, 2243-2248.
15. Y. S. Jung and C. A. Ross, *Nano Lett*, 2007, **7**, 2046-2050.
16. K. Fukukawa, L. Zhu, P. Gopalan, M. Ueda and S. Yang, *Macromolecules*, 2005, **38**, 263-270.
17. Z. Q. Lin, D. H. Kim, X. D. Wu, L. Boosahda, D. Stone, L. LaRose and T. P. Russell, *Adv Mater*, 2002, **14**, 1373-1376.
18. S. Kim, R. M. Briber, A. Karim, R. L. Jones and H. C. Kim, *Macromolecules*, 2007, **40**, 4102-4105.
19. R. M. Ho, W. H. Tseng, H. W. Fan, Y. W. Chiang, C. C. Lin, B. T. Ko and B. H. Huang, *Polymer*, 2005, **46**, 9362-9377.
20. W. A. Phillip, M. A. Hillmyer and E. L. Cussler, *Macromolecules*, 2010, **43**, 7763-7770.
21. M. F. Zhang, L. Yang, S. Yurt, M. J. Misner, J. T. Chen, E. B. Coughlin, D. Venkataraman and T. P. Russell, *Adv Mater*, 2007, **19**, 1571-+.
22. G. Riess, *Prog Polym Sci*, 2003, **28**, 1107-1170.
23. M. Faustini, G. L. Drisko, A. A. Letailleur, R. S. Montiel, C. Boissiere, A. Cattoni, A. M. Haghiri-Gosnet, G. Lerondel and D. Grosso, *Nanoscale*, 2013, **5**, 984-990.
24. J. P. Spatz, S. Sheiko and M. Moller, *Adv Mater*, 1996, **8**, 513-&.
25. T. Ghoshal, R. Senthamaraikannan, M. T. Shaw, J. D. Holmes and M. A. Morris, *Nanoscale*, 2012, **4**, 7743-7750.
26. M. K. Mayeda, J. Hayat, T. H. Epps and J. Lauterbach, *J Mater Chem A*, 2015, **3**, 7822-7829.
27. C. C. Chao, T. C. Wang, R. M. Ho, P. Georgopanos, A. Avgeropoulos and E. L. Thomas, *Acs Nano*, 2010, **4**, 2088-2094.
28. T. Li, Z. Wang, L. Schulte, S. Ndoni, *Nanoscale*, 2015, DOI: 10.1039/C5NR06815K.
29. T. Li, L. Schulte, O. Hansen and S. Ndoni, *Micropor Mesopor Mat*, 2015, **210**, 161-168.
30. S. Ndoni, P. Jannasch, N. B. Larsen and K. Almdal, *Langmuir*, 1999, **15**, 3859-3865.
31. J. W. Jeong, W. I. Park, M. J. Kim, C. A. Ross and Y. S. Jung, *Nano Lett*, 2011, **11**, 4095-4101.
32. T. Y. Lo, C. C. Chao, R. M. Ho, P. Georgopanos, A. Avgeropoulos and E. L. Thomas, *Macromolecules*, 2013, **46**, 7513-7524.
33. W. B. Bai, A. F. Hannon, K. W. Gotrik, H. K. Choi, K. Aissou, G. Liontos, K. Ntetsikas, A. Alexander-Katz, A. Avgeropoulos and C. A. Ross, *Macromolecules*, 2014, **47**, 6000-6008.
34. S. Rasappa, L. Schulte, D. Borah, M. A. Morris, S. Ndoni, *Coll. Interf. Sci. Comm.*, 2014, **2**, 1-5.
35. J. E. Mark, *Polymer data handbook*, 2nd edn., Oxford University Press, Oxford ; New York, 2009.
36. C. L. Yaws, *Thermophysical properties of chemicals and hydrocarbons*, Second edition. edn., 2014.
37. J. G. Son, K. W. Gotrik and C. A. Ross, *Acs Macro Lett*, 2012, **1**, 1279-1284.

38. V. V. Starkov, E. Y. Gavrilin, J. Konle, H. Presting, A. F. Vyatkin and U. Konig, *Phys Status Solidi A*, 2003, **197**, 150-157.
39. S. M. Kim, S. J. Ku, G. C. Jo, C. H. Bak and J. B. Kim, *Polymer*, 2012, **53**, 2283-2289.
40. S. J. Ku, G. C. Jo, C. H. Bak, S. M. Kim, Y. R. Shin, K. H. Kim, S. H. Kwon and J. B. Kim, *Nanotechnology*, 2013, **24**.
41. K. R. Williams and R. S. Muller, *J Microelectromech S*, 1996, **5**, 256-269.

Graphical Abstract:

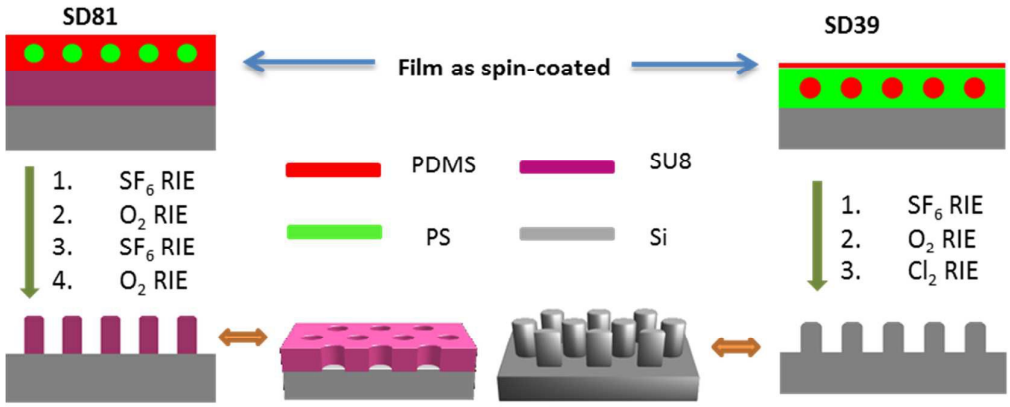

Fully scalable nanopatterning by direct PS-*b*-PDMS block copolymer lithography, without substrate pre-modification and without annealing.